# Tensile strain fields around an edge knot in a spruce specimen

*J. Oscarsson[1], A. Olsson[2] & B. Enquist[3]*

## Abstract

Strain fields around a traversing edge knot in a spruce specimen subjected to tensile loading were measured using a contact-free measuring technique based on digital image correlation. The strain fields were measured by consecutive load tests in which one side of the specimen was studied during each test. The objectives were to examine 1. to what extent the strain fields could be detected, 2. the correlation between strain fields on different sides of the specimen, and 3. the strain distribution around the knot. It was shown that the applied technique is very useful for catching both overall and detailed information about the behaviour of knots in wood members exposed to loading. Both clear wood defects that could not have been detected by visual inspection or scanning and the release of internal stresses were identified. The correlation between strain fields on different sides of the specimen was very good. The correspondence between measurement results and comparative finite element calculations was surprisingly good, considering the fact that the used model was fairly simple.

## 1 Introduction

Present day methods for machine strength grading of structural timber are based on somewhat limited relations between measured characteristics and predicted strength properties. The latter are to a large extent dependent on the occurrence of defects. The degree of importance that different defects have on strength and stiffness has been investigated by *e.g.* Johansson *et al.* (1998) and Johansson (2003). It was found that knots were by far the type of defects that had the largest influence on the grading and that the major cause of fracture was the presence of knots. Hence it follows that a thorough understanding of the behaviour of knots and surrounding wood fibres in timber members exposed to loading is of great importance for the development of more accurate grading methods. In this matter, techniques for contact-free strain measurement on timber surfaces could be very useful. One such method, today widely used in for example the vehicle and aviation industries, is based on white-light digital image correlation (DIC). The use of DIC in relation to wood is, however, limited. A review of research carried out up to the year of 2005 was presented by Serrano & Enquist (2005) who investigated strain distribution along wood adhesive bonds using DIC technique. A number of additional papers have been published in recent years (*e.g.* Young Jeong *et al.* 2009).

[1] PhD Student, jan.oscarsson@sp.se
SP Technical Research Institute of Sweden, Sweden
[2] Professor, anders.olsson@lnu.se
Linnæus University, Sweden
[3] Research Engineer, bertil.enquist@lnu.se
Linnæus University, Sweden

## 2 Aim and scope

In this paper, findings from an investigation of two-dimensional strain fields around a traversing edge knot (henceforth denoted *Edge knot*) in a Norway spruce test specimen, see Figure 1 (left), subjected to tensile forces were studied using a non-contact optical 3D deformation measurement system of white-light DIC type. The aims were to investigate 1. to what extent the strain fields could be detected, 2. the correlation between the strain fields measured on different sides of the specimen, and 3. the strain distribution around the knot. The development of strain fields were followed and measured by consecutive cyclic load tests consisting of both loading and unloading. Only one side of the specimen was studied during each test. Except for an initial test in which a crack in the knot widened and propagated, the loading was kept within the elastic range. Thus, the strain fields as function of load level were detected in a comparable manner on all four sides of the specimen even though only one side was studied during each test. The experimental results were also compared with those obtained from finite element (FE) simulations.

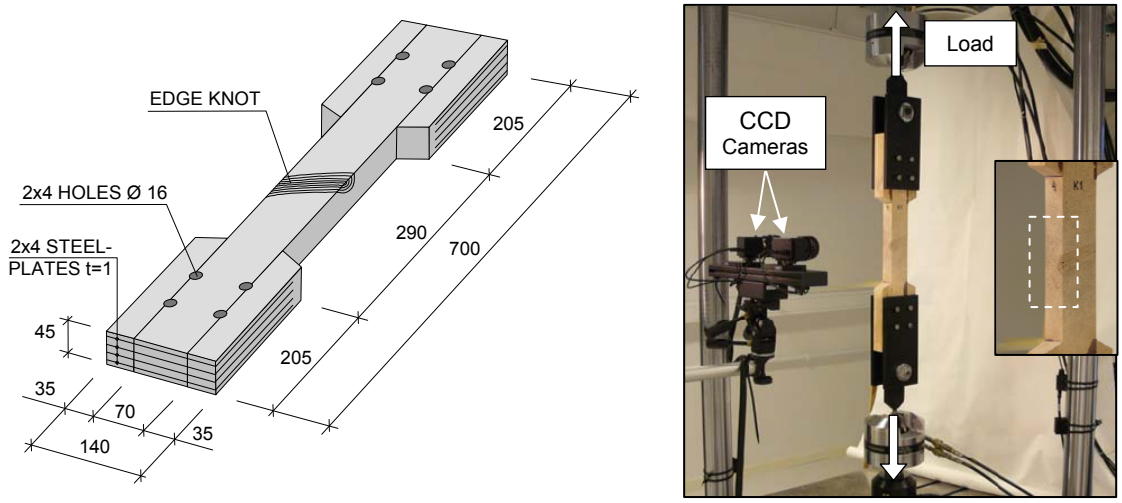


Figure 1: Test specimen (left); test setup with inset measurement area (right).

## 3 Test setup and measurement equipment

The test specimen was fixed by pin-ended steel yokes in a material testing machine of fabricate MTS, see Figure 1 (right), with a force capacity of ±100 kN. The applied cyclic load ranged from 0 to 30 kN, except for one test in which the maximum load was 40 kN. The two-dimensional strain fields in longitudinal and lateral directions and in shear occurring on the surfaces of the specimen were detected using the measuring system ARAMIS$^{TM}$, by which strains in the range of 0.05-200 % could be measured with an accuracy of up to 0.02 % strain (GOM 2007). It includes two Charge-Coupled Device (CCD) cameras, in this case with a resolution of 2048×2048 pixels. During loading, the surface deformations and displacements are recorded by pictures taken simultaneously, but from different angles, by the two cameras at fixed time intervals during the entire load test. From each pair of pictures, stereoscopic images are obtained and 3D-coordinates for a large number of points on the distorted surface are calculated relative to a coordinate system defined through a calibration

procedure prior to the test. In this research, pairs of pictures were taken at a time interval of two seconds, corresponding with a load increment of 400 N. Thus, a test with a maximum load of 30 kN consisted of about 150 load stages.

To be able to determine the displacements of a distinct point on the surface, each picture is divided into partially overlapping square or rectangular image sub-pictures, so called facets. The size in pixels of both facets and overlap could be adjusted due to the spatial resolution and measurement accuracy needed for the test in question. In this case, the system's default settings, which are square 15×15 pixel facets and two pixel overlap, see Figure 2 (left), were selected. This resulted in a facet step of 13 pixels, corresponding with a spatial resolution of about 0.67 mm. The default values are chosen as a compromise between measurement accuracy and computational time (GOM 2007). During a load test, each facet is identified for every subsequent stereoscopic image in the recording. This requires that the object's surface has an identifiable pattern, in this case a random speckle pattern of sprayed paint, see Figure 2 (middle). During a test, such a pattern deforms along with the surface distortion and by use of correlation algorithms, the 3D coordinates of a facet are calculated as the mean value of the coordinates of the facet corners. In Figure 2 (right), the facet coordinates of 9 facets are shown as red and blue dots. The coordinates also define and coincide with the measuring point of the facet. Displacements of the facet coordinates in a 3×3 facet mesh are used to calculate the strains in the measuring point (blue dot in Figure 2 (right)) of the centre facet of the mesh. By following changes in position of a large number of facets, the strain field as function of the load level can be determined and visualized.

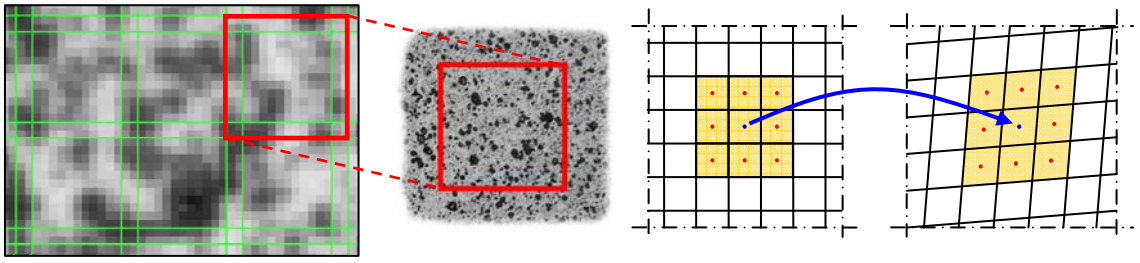

Figure 2: Pixel facets of size 15×15 pixels with a two pixel overlap (left), random pattern of a facet (middle), and facet mesh before and under loading (right).

## 4 Test specimen and loading

The experimental part of the research consisted of a test series in which the specimen was exposed to five load tests, numbered A0-A4. Considering the load eccentricity *e* of about 5.5 mm in the section through the knot, see Figure 3 (right), and in order to keep the stresses and strains within the elastic range, a maximum tension load of 40 kN was chosen, equal to an average tensile stress of 12.7 MPa. However, during the first load test (no. A0) an initial crack at the pith of the knot expanded and propagated to the full depth of the knot, see Figure 3 (right). Because of this, the load level was reduced to 30 kN for load tests no. A1-A4, in which the strains on the specimen surfaces were measured. The load application in all the tests was force controlled, which meant that the load was both applied and detached with a constant load rate of 200 N/second.

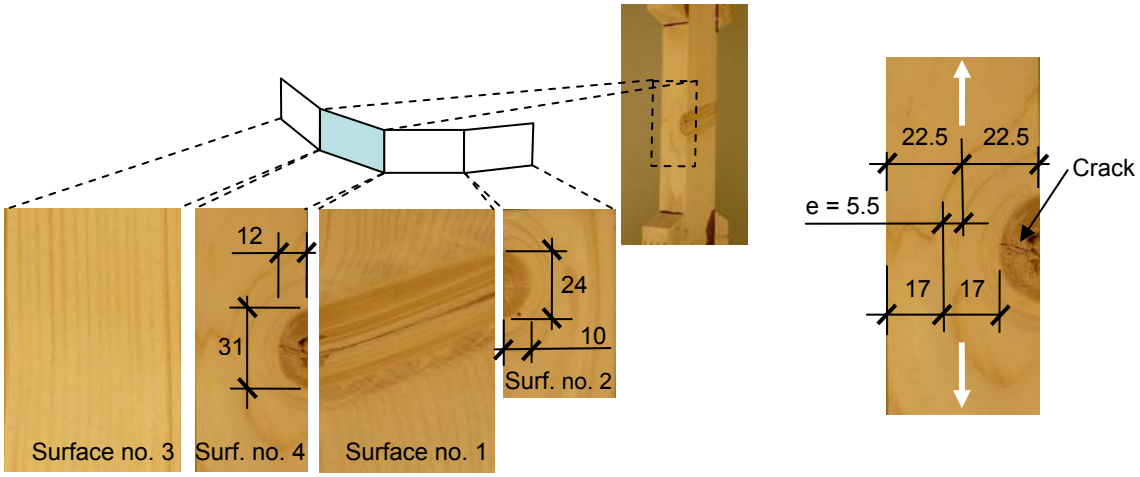


Figure 3: Knot dimensions (left), and load eccentricity *e* at Edge knot (right).

## 5 Test results and evaluations

Two ARAMIS™ post-processing tools, contour plots and section diagrams, were used to visualize the strain measuring results. By the first tool, a camera image of a measured surface is overlaid with coloured strain contour plots showing the strain distribution, for a defined load stage, over the surface. Such plots offer a qualitative and easily conceivable impression of the specimen's behaviour under loading. To obtain quantitative information with a higher degree of accuracy, sections, or paths, can be defined in surface camera images and the strain variation along such sections can be shown in section diagrams.

### 5.1 Load test no. A0: Load 40 kN

As described under heading *4. Test specimen and loading*, a tension load of 40 kN was chosen for this test in which the strains on the specimen surface that shows a split section of the knot (Surface no. 1, see Figure 3) were measured. Longitudinal strains ($\varepsilon_y$) for certain load stages are presented in Figure 4. Stages no. 0-4 represent the undeformed and unloaded reference state and the specified load level of 0.10 kN is considered as measuring noise.

Load stages no. 102-105 illustrate the load stages just before and after the maximum load level of 40.1 kN was reached at stage no. 103. At this load, the crack had propagated and widened to such an extent that it was no longer possible to identify and follow displacements and deformations of facets in the crack area by means of the random surface pattern of sprayed paint. Surface points that were not possible to identify are shown as holes in the contour plots, see detail in Figure 4. During the unloading phase the crack was gradually closed and the pattern restored to a degree where the facet displacements across the crack area were again possible to measure. However, considerable deformations, shown as a thick red stripe in the contour plot of the last load stage (no. 203), remained in the crack after completed unloading.

Large remaining negative (compressive) strains appeared in the wood fibres quite close to the knot. In general, strain changes measured by the ARAMIS™ system from one load stage to another are rather small and more or less

foreseeable, but in this test the negative strains along the knot appeared instantly, at load stage no. 104, immediately after the maximum load of 40.1 kN was reach. In load stages no. 102 and 103 rather small negative strains were discerned in the wood fibres just above the knot whereas distinct tensile strains had developed below the same. During the two seconds that elapsed between the moments when pictures of load stages 103 and 104 were taken, the strain field around the knot was completely changed and large areas of considerable negative strains emerged. A part of these remained after unloading, see load stage no. 203. After the test and by use of a pocket lens, three longitudinal cracks were discernible on Surfaces no. 2 and 4. One was situated at the knot edge and two in the clear wood close to the knot. The cracks are highlighted in the section diagrams of Figures 5-6 recorded for load tests A1-A4. A reasonable explanation to the sudden strain field changes is that crack growth during the test led to the release of internal stresses. It should also be noted that the stress release occurred between the load stages no. 103 and 104, *i.e.* just after the maximum load level was reached. This indicates that the release was, to some extent, triggered by the change of sign of the load increment of 200 N/s.

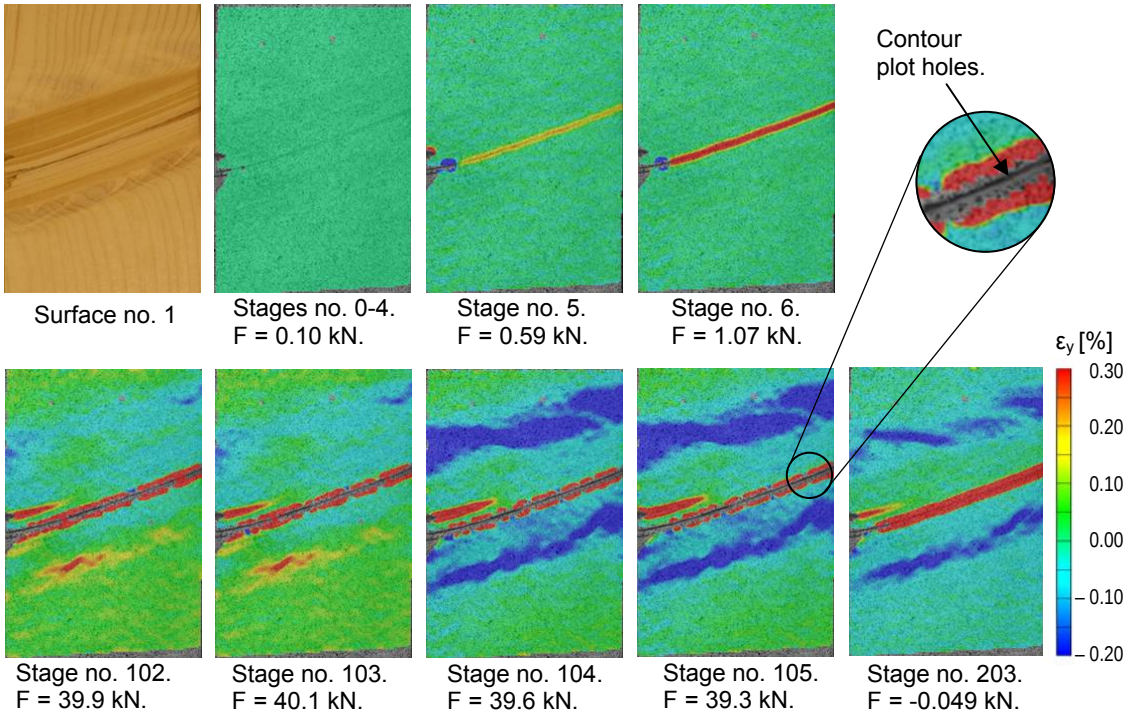


Figure 4: Contour plots for longitudinal strains ($\varepsilon_y$) on Surface no. 1, Load test no. A0, Load stages no. 0-6, 102-105 and 203.

## 5.2 Load test no. A1-A4: Load 30 kN

In tests no. A1-A4, in which the final strain stage of test no. A0 was used as undeformed and unloaded reference stage (stage 0), the specimen was exposed to a tension load of 30 kN for which an elastic behaviour was displayed. Contour plots and section diagrams referring to the load stage for which the maximum load 30 kN was reached are shown in Figures 5-6. The most conspicuous feature of the contour plots was the strain concentrations in

the wood fibres close to the knot. In spite of the fact that the specimen was exposed to tension loads, significant longitudinal negative strains were visible on Surfaces no. 1 and no. 3, see Figure 5. The minor longitudinal negative strains in Section y = – 40 mm on Surface no. 3 are explained by the load eccentricity *e* that according to Figure 3 (right) occurred in the specimen. The three strain peaks ($\varepsilon_y \geq 0.4$ %) in the section diagrams for Surfaces no. 2 and 4 in Figure 5 are related to the previously described longitudinal cracks that were observed by use of a pocket lens. What is measured and interpreted as surface strain peaks are in fact displacements caused by gradual widening of the cracks as load is applied. The local tensile strain of about 0.82 % registered at Section y = – 40 mm on Surface no. 1 was also caused by the widening of a crack, in this case located within the knot and shown as a red stripe in the contour plot.

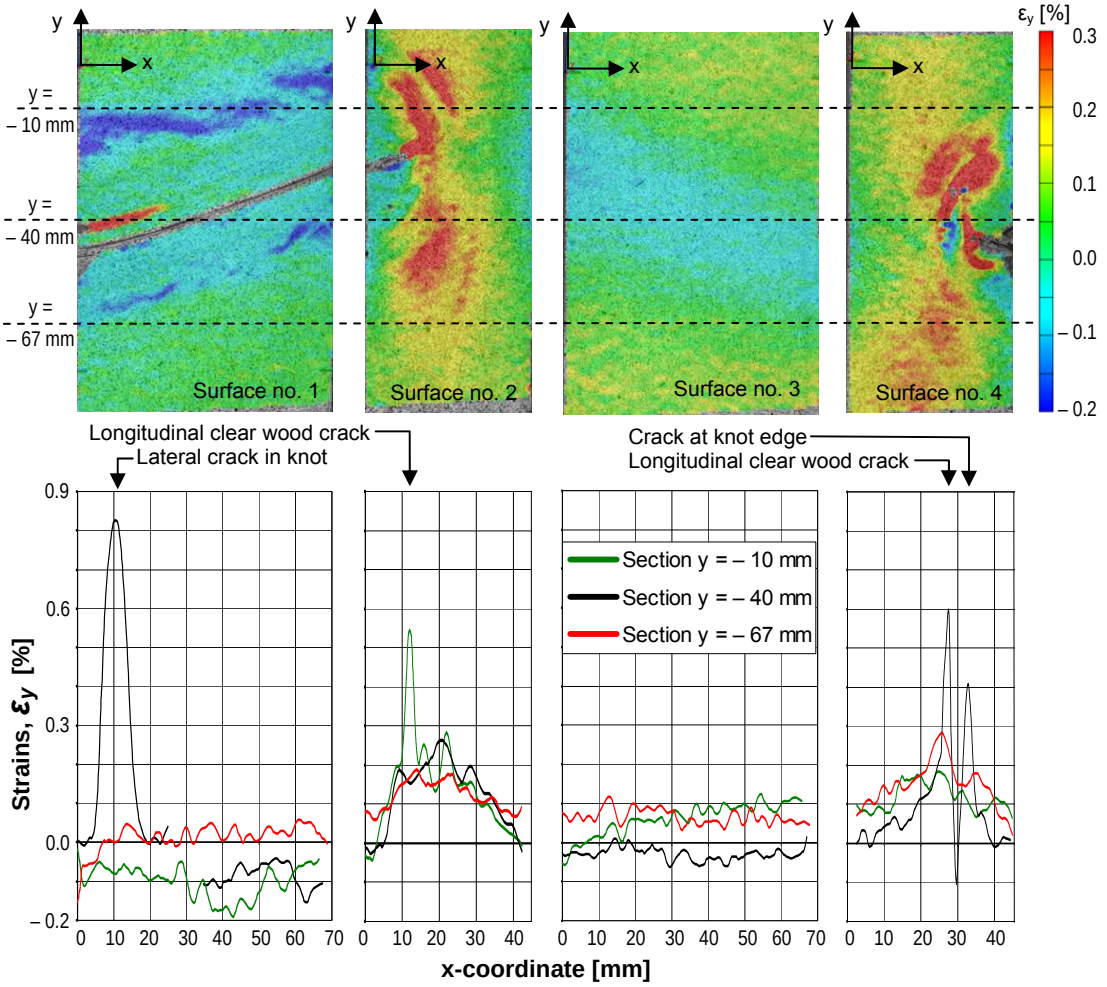


Figure 5: Longitudinal surface strains ($\varepsilon_y$) for maximum load 30 kN, recorded for Load tests no. A1-A4. Top row: Contour plots. Bottom row: Section diagrams for the sections (dashed lines) shown in the top row.

The lateral strains measured in Load tests no. A1-A4 are shown in Figure 6. They were insignificant on Surface no. 1, since the contraction was prevented by the presence of the knot. From a comparison of the contour plot of Surface no. 3 in Figure 6 and the corresponding surface photo in Figure 3, a correlation

between the annual ring width and the wave-like pattern of the plot can be observed. This indicates a difference between Poisson's ratios in early wood and late wood for Norway spruce. Such a difference has been observed for loblolly pine (Young Jeong *et al.* 2009). On Surfaces no. 2 and 4, large lateral tensile strains developed close to the knot. They are shown as red areas in the contour plots in Figure 6. However, the huge apparent strains that coincide with the previously described cracks highlighted in the section diagrams in Figure 6 are in fact lateral displacements caused by widening of the cracks.

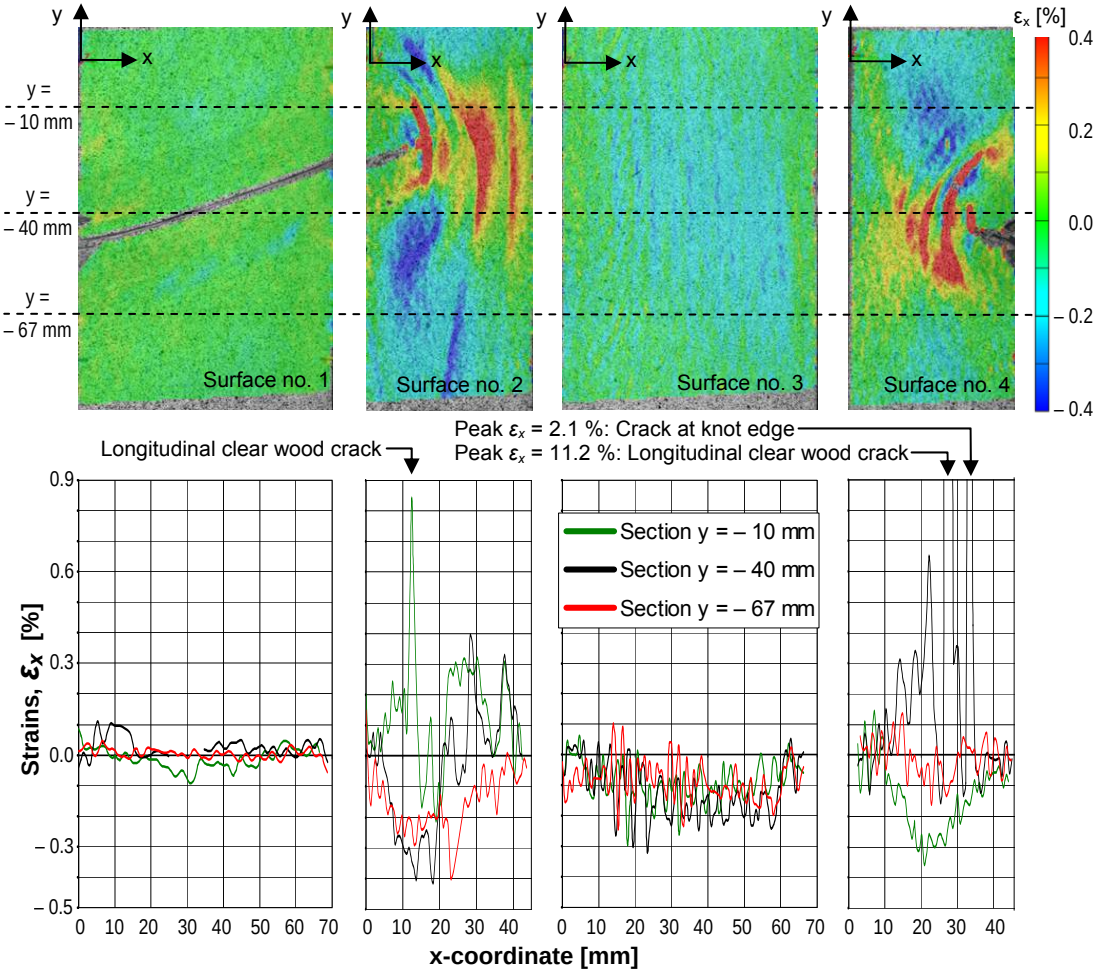


Figure 6: Lateral surface strains ($\varepsilon_x$) for maximum load 30 kN, recorded for Load tests no. A1-A4. Top row: Contour plots. Bottom row: Section diagrams for the sections (dashed lines) shown in the top row.

## 6 Numerical analyses

The results of the experiments were compared with those obtained from FE simulations using the ABAQUS FE software (ABAQUS 2008). In the FE calculations, a 3D linear elastic model of the specimen's behaviour under loading was used. The model comprised about 113000 elements and 483000 nodes resulting in 1449000 degrees of freedom.

The material data needed for the numerical calculations, expressed in terms of elastic constants for spruce with a moisture ratio of 12 %, were obtained from

Kollman & Côté (1968). The constants used for both clear wood and knot were $E_L$ = 13500, $E_R$ = 893, $E_T$ = 481, $G_{LR}$= 716, $G_{LT}$ =500 and $G_{RT}$ =29 MPa for the moduli of elasticity and the shear moduli, and $v_{LR}$ = 0.43, $v_{LT}$ =0.53 and $v_{RT}$ = 0.42 for Poisson's ratios. The indices L, R and T refer to the longitudinal, radial and tangential directions, respectively, of the modelled orthotropic wood material. The longitudinal direction of the clear wood was oriented parallel with the longitudinal direction of the specimen, whereas the longitudinal direction of the knot was oriented perpendicular to the mentioned clear wood direction.

The applied FE model was fairly simple. The crack that widened and propagated in the pith of the knot during load test no. A0 was included, but the material orientation deviations that always occur in clear wood close to knots were not regarded. Nevertheless, the simulation results presented in Figures 7 show, on an overall and qualitative level, a degree of correspondence with the experimental results in Figures 5-6 that is surprisingly good. In terms of strain features on a closer level, it should be noted that the longitudinal negative strains measured on Surface no. 1, see contour plot in Figure 5, also could be found on the corresponding plot in Figure 7. The most conspicuous differences between measured and calculated strains concern the large apparent tensile strains, both longitudinal and lateral, which occurred close to the knot, see Figures 5-6. These apparent strains, which in fact were displacements caused by the cracks that were identified by use of a pocket lens, could not be seen in the results of the simulations since these cracks were not included in the model.

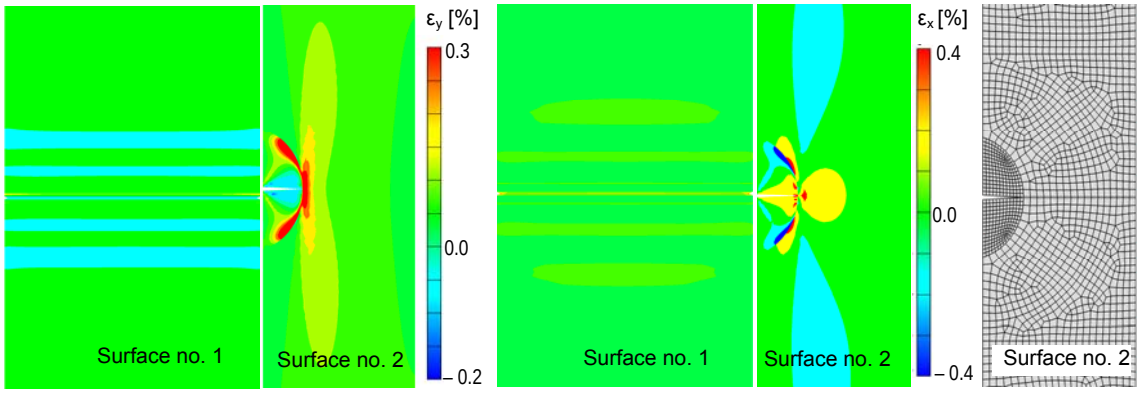


Figure 7: Results from FE simulation: Longitudinal strains (left), Lateral strains (middle) and FE mesh (right).

## 7 Conclusions and future work

The objectives of this research were to investigate to what degree strain fields around a knot could be detected by use of DIC technique, to analyse the strain distribution around the knot and to examine the correlation between strain fields measured on different sides of a test specimen. Regarding the two first objectives, it could be concluded that the DIC technique is a very useful tool for catching both qualitative and quantitative information about the behaviour of knots in wood members exposed to loading. The observation of release of internal stresses close to the knot must be considered as rather interesting. The graphical representations of the strain measuring results by use of contour plots

and section diagrams for all load stages in a load test provide valuable information about the strain distribution and development around knots. It is also possible to detect clear wood defects that are difficult to identify otherwise. For example, the three cracks on Surfaces no. 2 and 4 of the specimen could not have been detected neither by scanning nor visual inspection. It is very likely that the cracks will serve as indications of fracture and in the plans for future work, a fracture test of the specimen is included. In such a test, the progress of fracture will be documented by use of the ARAMIS™ system.

With reference to the objective concerning correlation between strain fields on different specimen surfaces, it has been demonstrated that the strain match between adjacent sides is very good, taken into account that only one specimen surface was measured during each load test.

Finally, the correspondence between measurement results and FE simulations are indeed very promising, especially considering the fact that the applied model was rather simple. The DIC technique used in this research will, with a high degree of probability, be of great interest for calibration of finite element models for analyses of fracture mechanical behaviour of knots in wood members. Such models would be of great importance for the development of more accurate strength grading methods based on scanned information concerning the occurrence of knots liable to initiate fractures in wood members.

## References

ABAQUS Inc (2008) "ABAQUS/CAE Version 6.8, User's Manuals".

GOM mbH (2007) "ARAMIS User Manual – Software". aramis_v6_1st_en_rev-c, 25-Apr-2007.

Johansson, C.-J., Boström, L., Bräuner, L., Hoffmeyer, P., Holmquist, C. & Solli, K. H. (1998) "Laminations for glued laminated timber – Establishment of strength classes for visual strength grades and machine settings for glulam laminations of Nordic origin". SP Swedish National Testing and Research Institute, SP REPORT 1998:38.

Johansson, C.-J. (2003) "Grading of timber with respect to mechanical properties". In S. Thelandersson and H. J. Larsen, editors, Timber Engineering, pp 23-43. John Wiley & Sons Ltd, Chichester, England.

Kollman, F.F.P., Côté, W.A. (1968) "Principles of Wood Science and Technology". Springer Verlag, Berlin Heidelberg, Germany.

Serrano, E. & Enquist, B. (2005) "Contact-free measurement and non-linear finite element analyses of strain distribution along wood adhesive bonds". Holzforschung, Vol 59, pp 641-646.

Young Jeong, G., Zink-Sharp, A. & Hindman, D. P. (2009) "Tensile properties of earlywood and latewood from Loblolly Pine (Pinus Taeda) using Digital Image Correlation". Wood and Fibre Science, Vol 41, No 1, pp 51-63.